DEFENCE
SCIENCE & TECHNOLOGY

May 2003

DSTO

Experimental Verification of Helicopter-Rotor Loads-Synthesis Models

Frank G. Polanco, Chris G. Knight, Scott A. Dutton, and Phil Ferrarotto

DSTO-TR-1428

DEFENCE
SCIENCE & TECHNOLOGY

Experimental Verification of Helicopter-Rotor Loads-Synthesis Models

Frank G. Polanco, Chris G. Knight, Scott A. Dutton, and Phil Ferrarotto

Air Vehicles Division
Platforms Sciences Laboratory

DSTO–TR–1428

ABSTRACT

Accurately synthesising the load in helicopter-rotor components, using measurements taken from fixed components, has the potential to increase safety and reduce operating costs. Two synthesis models, one of which is able to handle noisy and collinear environments, were validated using data from a Eurocopter Squirrel gearbox fitted to DSTO's Helicopter Transmission Test Facility. The aim of the experiment was to test the models under "challenging" conditions—namely, a noisy and collinear measurement environment. Despite the synthesis techniques being validated, the testing environment did not prove challenging enough (mainly due to insufficient collinearity between the strain gauges). Both the instrumental variable (IV) and least squares (LS) models were able to synthesise the required loads to a high degree of accuracy. The IV model (unlike the LS model) was found to be very sensitive to the chosen gauge combination.

Published by

DSTO Platforms Sciences Laboratory
506 Lorimer St,
Fishermans Bend, Victoria, Australia 3207

Telephone: *(03) 9626 7000*
Facsimile: *(03) 9626 7999*

AR No. AR–012–759
May, 2003

APPROVED FOR PUBLIC RELEASE

Experimental Verification of Helicopter-Rotor Loads-Synthesis Models

EXECUTIVE SUMMARY

In terms of fatigue cracking, critical components in helicopters differ in two significant ways from equivalent components in fixed-wing aircraft: these critical components (i) are usually part of a single load path and (ii) are subjected to both high and low frequency loading. The high frequency loading means that cracks usually propagate quickly, with the resulting potential for catastrophic failures because of the single load path.

Most of these critical components have a specified component retirement time (CRT), which the manufacturer bases on an assumed usage spectrum, with associated component loads determined either analytically or from one-off flight tests. The Australian Defence Force (ADF), however, operates most of its aircraft in a manner different to that initially envisaged by the manufacturer, and often with configurations different from the manufacturer's test aircraft. These different spectra mean that some components may be experiencing a heavier usage than originally anticipated, which has safety implications for the operator. Conversely, other components will be retired at their CRT with a large portion of useable life still intact, which has cost implications for the operator. Thus the accurate determination of loading on critical rotating components has both safety and cost saving benefits for the ADF.

One method of determining these component loads during flight is to directly measure them using strain gauges. Due to the harsh working environment, however, gauges mounted directly on these critical rotating components tend to be short-lived. Furthermore, there is also the problem of data recovery from these directly mounted gauges. The two historical procedures used for this recovery are themselves problematic: telemetry is plagued by noisy signals and in situ storage devices have limited data-storage capacity.

A loads-synthesis model, which uses information from gauges on fixed components to synthesise the load in rotating components, overcomes the problems of gauge life and data transfer. In this report we validate two loads-synthesis models (developed earlier) using the Helicopter Transmission Test Facility (HTTF) located at DSTO's Melbourne site.

The HTTF was chosen because it was relatively cheap, timely, and easy to obtain experimental results. A strain gauged Eurocopter Squirrel gearbox was used in the HTTF for testing. Five gross loads (two lift loads, two drag loads, and torque) were applied to the gearbox and recorded along with the resulting output from ten strain gauges attached to static portions of the gearbox. The loads were applied as quasi-dynamic steps for approximately forty minutes. The resulting data set obtained from this experiment was used to validate the loads-synthesis models.

The aim of the experiment was to test the models under "challenging" conditions—namely, noisy measurements and gauge collinearities. Two models were examined: a simple least squares (LS) model and a more sophisticated instrumental variable (IV) model. Unfortunately, the chosen geometry of the gearbox gauges turned out to be anything but collinear resulting in a test case that was not challenging enough. Both models were able

to accurately and easily synthesis the five gross loads applied to the gearbox. However, the IV model was very sensitive to the gearbox gauge combination. Using the wrong combination of gauges in the IV model led to errors that were more than two orders of magnitude larger than errors from the IV model with the best gauge combination.

Authors

Frank G. Polanco
Air Vehicles Division

Frank Polanco graduated in 1992 with a Bachelor of Aerospace Engineering (Honours) and a Bachelor of Applied Science (Distinction) from the Royal Melbourne Institute of Technology (RMIT). He joined the Platforms Sciences Laboratory (PSL) in 1993, working on aircraft structural integrity and fatigue life monitoring before returning to RMIT to complete a Doctorate in Mathematics. He then rejoined the PSL in 1998 to work in the area of helicopter life assessment. At PSL he has worked on: loads synthesis of helicopter-rotor component, fatigue and cost effects of spectrum perturbations, component reliability, and measures for vibrational modes.

Chris G. Knight
Air Vehicles Division

Mr Chris Knight is an engineer in the Helicopter Life Assessment area of Air Vehicles Division at the Platforms Sciences Laboratory (PSL). He joined PSL in 1994 after graduating from the University of NSW with a Bachelor of Aerospace Engineering degree with honours. His work has included flight test investigation of S-70A-9 Black Hawk cracking problems and design and testing of an improved Fast Roping and Rappelling Device. In 1997 he left PSL to work in Seattle for the Boeing Commercial Aircraft Group. He returned to PSL in 1999. Since his return his work has included an examination of cracking in the UH-1H Iroquois vertical fin and a study into the effectiveness of Flight Data Recorders for usage monitoring.

Scott A. Dutton
Air Vehicles Division

Since graduating in 1985 with an Electrical Engineering degree, Scott Dutton has worked at the Platforms Sciences Laboratory primarily in the field of instrumentation and data acquisition in both test cell and flight trial environments. He has extensive experience with sensors and digital systems particularly for use in data acquisition and control systems. Flight trial work has included numerous trials on helicopters and fixed-wing aircraft. He has provided data acquisition and control systems for numerous test cells, primarily for vibration and engine performance monitoring. He is currently developing pneumatic control systems for full scale fatigue tests.

Phil Ferrarotto
Air Vehicles Division

Mr Phil Ferrarotto joined the Platforms Sciences Laboratory as an Electronic Engineer in 1973. He has worked in the area of strain gauge application and data acquisition since 1982.

Contents

1 Introduction **1**

2 Description of the Experimental Setup **4**

3 Description of the Testing Program **10**

4 Results **17**

5 Conclusion **26**

References **28**

Figures

1.1 Front-view photograph of Helicopter Transmission Test Facility 3
2.1 Side-view schematic of Helicopter Transmission Test Facility 5
2.2 Squirrel's dog-bone experiences mostly tensile loading 6
2.3 Squirrel gearbox and close-up photograph of strain-gauge rosette 7
2.4 Strain response of gearbox-casing rosette to applied torque 8
2.5 Photographs of strain gauged strut and dog-bone 9
3.1 Example of file re-alignment algorithm 12
3.2 Relative error in temporal re-alignment of partitioned files 13
3.3 Time history sample of re-alignment (using Horizontal Force 1 data) 14
3.4 Time history plots of raw voltage measurements for fifteen outputs 15
4.1 Time history plots of IV and LS synthesis compared to measured results . . . 18
4.2 Plots of IV error to LS error ratio 21
4.3 Error in LS loads synthesis of measured parameters 23
4.4 Statistical distribution of error versus number of input parameters 24

Tables

3.1 Helicopter Transmission Test Facility operating limits for Squirrel gearbox . . 10
3.2 Thirty-five load cases applied to gearbox 11
4.1 Numbering code used for input and output parameters 17
4.2 Errors for worst and best performing LS and IV synthesis 19

1 Introduction

An accurate loads-synthesis model for rotating components on helicopters has two main benefits for aircraft operators, including the Australian Defence Force (ADF): an increase in safety and a reduction in operating costs.

Most critical helicopter components have a component retirement time (CRT), which the manufacturer bases on an assumed usage spectrum. The ADF, however, operates its aircraft in a different manner than that initially envisaged by the manufacturer. The question then naturally arises: Under this different spectrum, will any of the critical components in a helicopter fail before their CRT? Unlike fixed-wing aircraft, helicopter components are normally part of a single load path and are subjected to both high and low frequency loading. Thus even a small crack in a critical component could quickly lead to a catastrophic failure resulting in the loss of the crew, the passengers, and the helicopter. Accurately synthesising the loading in critical rotating components would allow a more accurate determination of the component's life. Additionally, this same synthesis model could be used as a fault warning system (provided a small amount of redundancy was built into the model).

At the other end of the usage spectrum, some components will be retired at their CRT with a large portion of useable life still intact. This early retirement of useable components has cost implication for the operator.

Due to the harsh operating environment, gauges mounted directly on rotating components are short-lived. There are also problems with information recovery from directly gauging rotating components. Two solutions to this information recovery problem have been attempted: telemetry (which is plagued by noise) and in situ storage (which can only store a small amount of data). For a review of the component load estimation problem see Polanco [6].

There are two reasons why we concentrated on rotating components only (that is, fixed components were not modelled). First, a review by Lombardo [5, p. 46] has shown that most fatigue-critical components in helicopters are located in the rotor system and its drive train. Second, we have already noted that most of these components are part of a single load path in helicopters, and hence are critical components.

The synthesis aims to determine the relationship between loads experienced by the rotating components with loads measured on the fixed components. As a first step the load synthesis models that were developed are linear. Consider a simple example where x_1, x_2, and y represent the load on two fixed components and one rotating component, respectively. We could then develop a model of the form $y = c_1x_1 + c_2x_2$, where c_1 and c_2 are the two coefficients we are trying to determine using experimental (and, in the future, flight trial) measurements. The models take into consideration noise in the measurements and linear dependence between x_1 and x_2. For more information on the development of the loads-synthesis models see the two reports by Polanco [7, 8].

The main aim of this experiment was to test how well the synthesis models perform under challenging conditions. By "challenging" we mean that measurements are noisy

and that the measurements taken on the fixed components are almost linearly *dependent.*[1] The noise sources are both electronic and, due to vibration, mechanical. We chose to test the models under these challenging circumstances because we envisage that these would be the conditions encountered by any final aircraft-implemented system.

The Helicopter Transmission Test Facility (HTTF), located at DSTO Melbourne, was chosen to validate the loads-synthesis models for several reasons. The testing on the HTTF was relatively cheap, timely, and easy because the HTTF was already operational and on-site. (See Figure 1.1 for a photograph of the HTTF.)

Two gearboxes were available for testing in the HTTF: the Kiowa (Bell 206B) gearbox and the Squirrel (Eurocopter AS350) gearbox. The Squirrel's gearbox (shown in Figure 1.1) was chosen for testing so as to fit in with other testing programs being undertaken on these gearboxes in the HTTF.

As a first step, this experiment investigated how well the model synthesised quasi-dynamic loads. By quasi-dynamic loads we mean gross loads (torque, horizontal loads, and vertical loads) applied to a rotating rotormast head. Several different loading combinations were tested, and for convenience these loads were applied in a step fashion between these different combinations. The synthesis model was tested on the response to these loads. Although the rotormast was rotating, the loading within the step portion was almost static, hence the "quasi-dynamic" nomenclature.

During this experiment, the loads applied to the Squirrel gearbox differed from the loads a gearbox in flight would experience in several important ways. The true dynamic effects of a helicopter rotor response were not modelled. For example, a control stick input to the rotorhead would result in a dynamic response; whereas we have (in essence) only applied static loads. In future experiments a more realistic loading scenario (including dynamic rotor response simulations) will be applied.

[1]By linearly *dependent* we mean that at least one fixed-component measurement can be expressed as a linear combination of the remaining fixed-component measurements. In developing a loads-synthesis model we need to solve a system of equations constructed from these fixed-component measurements. If the measurements are linearly *dependent* then this system's solution would involve the inversion of a singular (or close to singular) matrix, which would result in large errors.

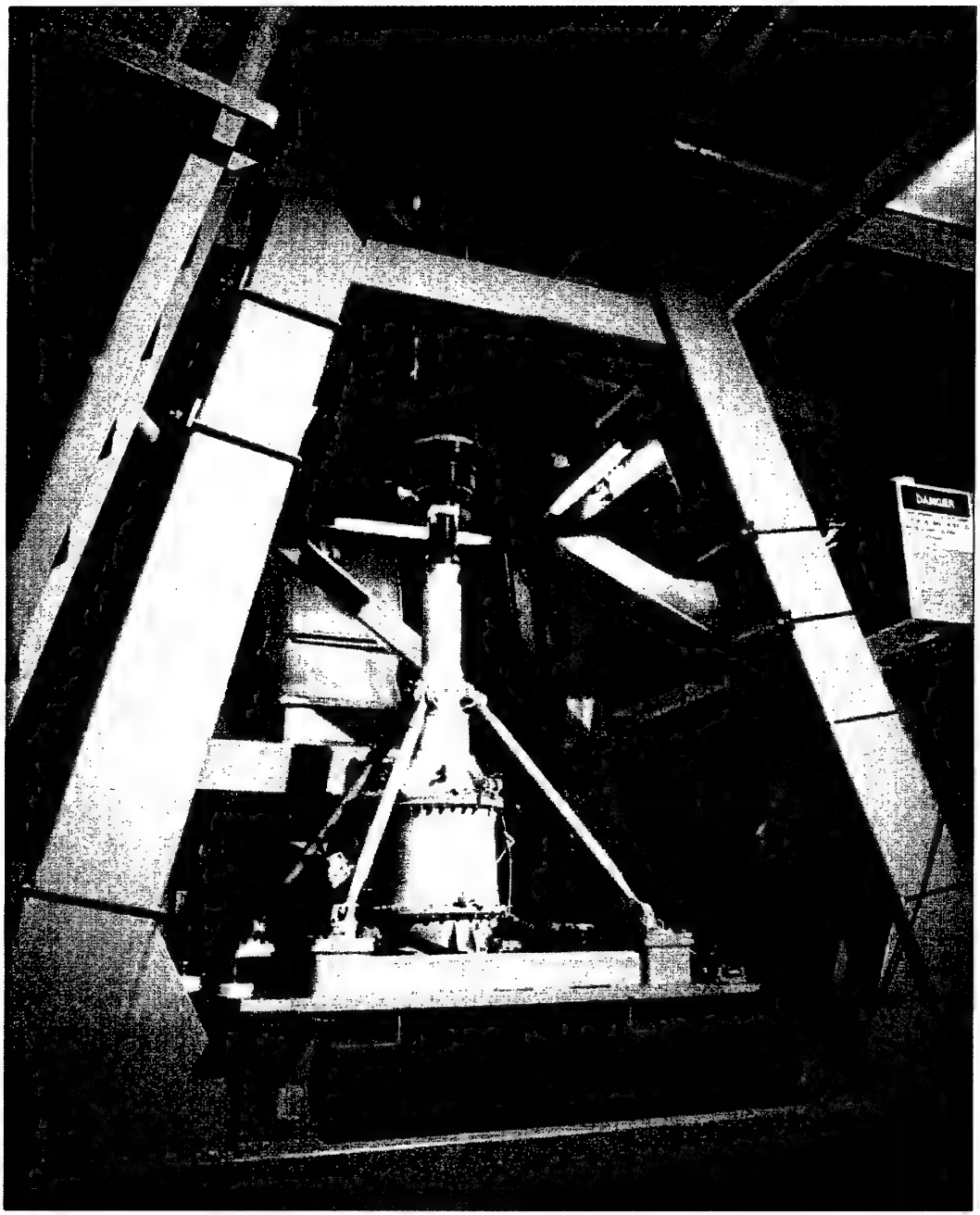

Figure 1.1: Front-view photograph of the Eurocopter Squirrel gearbox fitted into the Helicopter Transmission Test Facility. This photograph was taken prior to the gearbox's strain gauging. (Photograph kindly provided by the Boeing Applied Imaging Group.)

2 Description of the Experimental Setup

In this section we describe the experimental rig, the loads we wanted to synthesise, the easily measured loads, and the strain gauge locations for the easily measured loads.

Figure 2.1 shows a side-view schematic of the experimental rig, which was the Helicopter Test Transmission Facility (HTTF) located at DSTO Melbourne. An electric motor drives the gearbox (via the drive shaft), which is connected to the rotormast. In order to load the gearbox, the rotormast head is connected to a generator. The generator is not shown in this figure.

The gearbox is suspended by four struts (suspension bars); the side view in Figure 2.1 obscures two of these four struts. These struts were designed to insulate the gearbox from the lift force generated by the helicopter's main rotor. Thus the gearbox experiences mainly torsional load—which is reacted out to the airframe via the dog-bone (see Figure 2.2)—and also experiences some bending [1].

The left-hand side of Figure 2.1 represents the front of the gearbox, and hence the direction of forward flight. Looking from above, the Squirrel's rotor blades advance in a clockwise direction (that is, in the opposite direction to θ positive). The inset box in Figure 2.1 shows the direction of positive loading for the four load actuators superimposed onto a perspective view of the HTTF.

In a real helicopter, the loads we want to simulate are found on rotating components, while the loads we can easily measure are found on fixed components.

In this experiment, the five gross loads we simulated can be seen at the top of the rotormast in Figure 2.1 (and are shown in green). These loads are the two horizontal forces, the two vertical forces, and the rotormast torque (Q). The two load actuators that apply horizontal loads are labelled h_1 and h_2, and the two load actuators that apply vertical force are labelled v_1 and v_2. As is shown in Figure 2.1, the two horizontal loads are orthogonal to each other.

The easily measured loads, in this experiment, can be seen on the gearbox in Figure 2.1 (and are shown in red). The ten strain gauges attached to the gearbox are labelled "strain gauge", "gearbox rosette", and "dog-bone sets".

The main aim of this testing program was to investigate the effect of ill-conditioned inputs and high noise-to-signal ratios on the loads-synthesis results. By *ill-conditioned inputs* we mean inputs that are difficult to untangle (or resolve) using measurements.

In order to achieve this aim of ill-conditioned inputs, several (what were presumed to be) correlated gauge positions were chosen. For example, it was presumed that the tensile force on the four struts would be highly correlated.

Similarly, some gauge locations were chosen to obtain mildly high noise-to-signal ratios. For example, from the design of the gearbox's load path it was thought that the dog-bone would mainly experience tensile forces, with very little vertical or horizontal bending. The ends of the dog-bone take out some of the bending moments experienced by the gearbox; while lift loads are taken out by the struts (see Figure 2.1). The gearbox under torsional loading is shown in Figure 2.2. As can be seen, the torsional load Q on the gearbox is taken out through the dog-bone by the tensile load T. This tensile load should be the

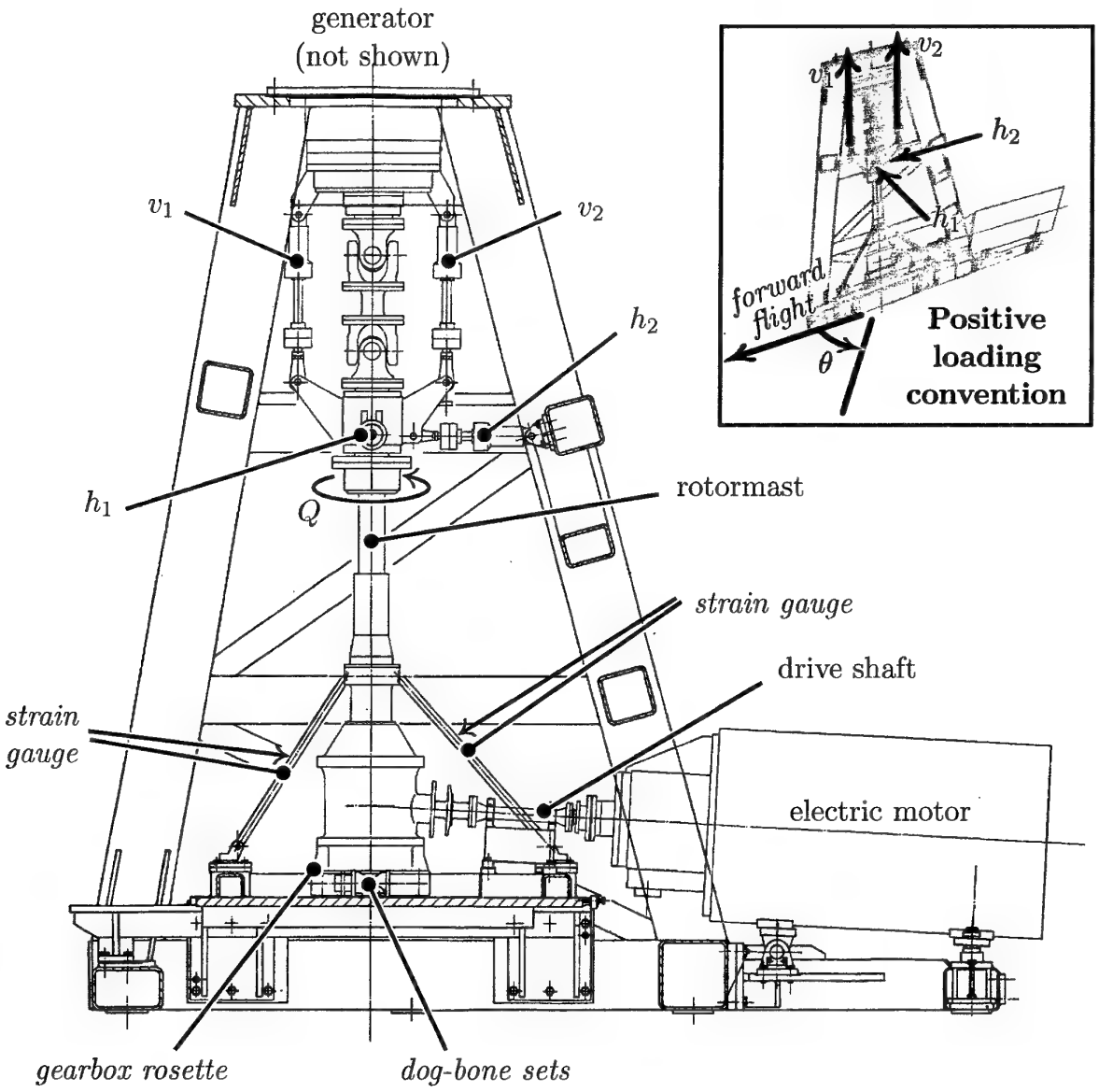

Figure 2.1: Side-view schematic drawing of the Helicopter Transmission Test Facility, with strain gauges labelled. The labels h_1, h_2, v_1, and v_2 denote the two horizontal and two vertical load actuators, respectively. The rotormast torque is denoted by Q. Each strut has one strain gauge, the gearbox has a rosette of strain gauges, and dog-bone has three sets of gauges (horizontal and vertical bending and tension-compression gauges). The inset box shows the positive sense of the applied loading and the direction of forward flight.

predominant load the dog-bone experiences. Thus measurements of both vertical and horizontal bending loads on the dog-bone should yield high noise-to-signal ratios.

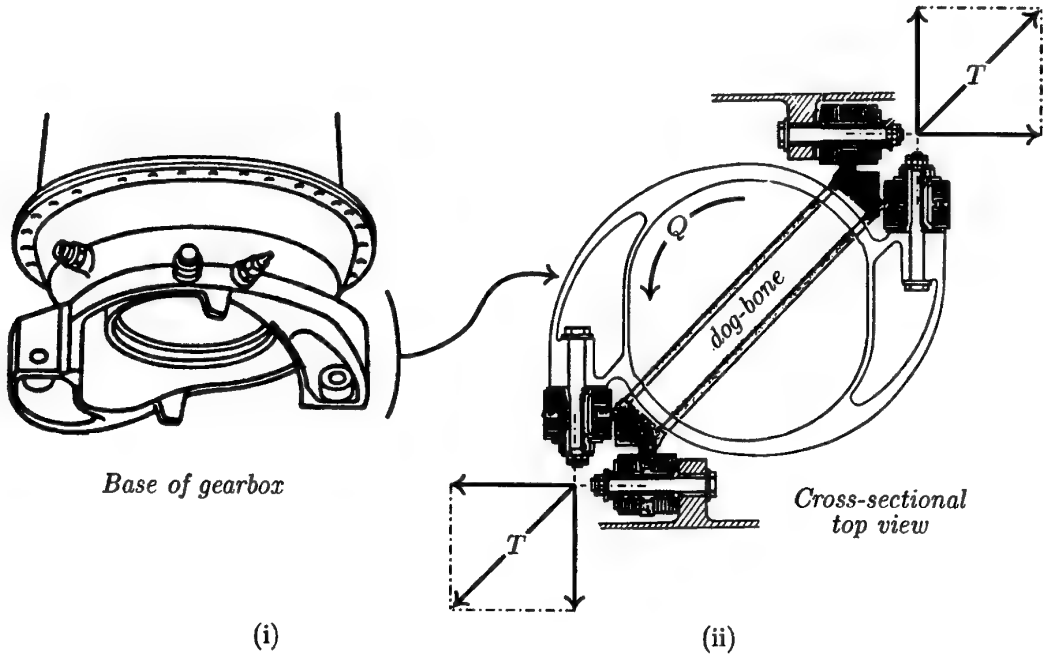

Figure 2.2: The dog-bone was designed to take loading mainly in tension. Part (i) shows the base of the gearbox (without the dog-bone). Part (ii) shows a cross-sectional top view of the dog-bone attached to the base of the gearbox, which is under torsional load. (Schematic adapted from Squirrel's instruction manual [1].)

And finally, although the strain gauge rosette was mounted on the gearbox casing near a mounting bolt, the casing itself in this region is thick. Due to this thick casing, it was presumed that only small strain readings would be recorded—again leading to a high noise-to-signal ratio.

In total, ten strain gauges were attached to the gearbox in the HTTF:

- one strain-gauge bridge (Micro Measurements CEA-13-062UT-350) on each of the four struts, see Figure 2.5(i);
- one horizontal-bending bridge (consisting of two strain gauges, both Micro Measurements EA-13-125BZ-350) on the dog-bone, see Figure 2.5(ii);
- one vertical-bending bridge (consisting of two strain gauges, both Micro Measurements EA-13-125BZ-350) on the dog-bone, see Figure 2.5(ii);
- one tension-compression bridge gauge (consisting of two strain gauges, both Micro Measurements CEA-13-125UT-350) on the dog-bone, see Figure 2.5(ii); and

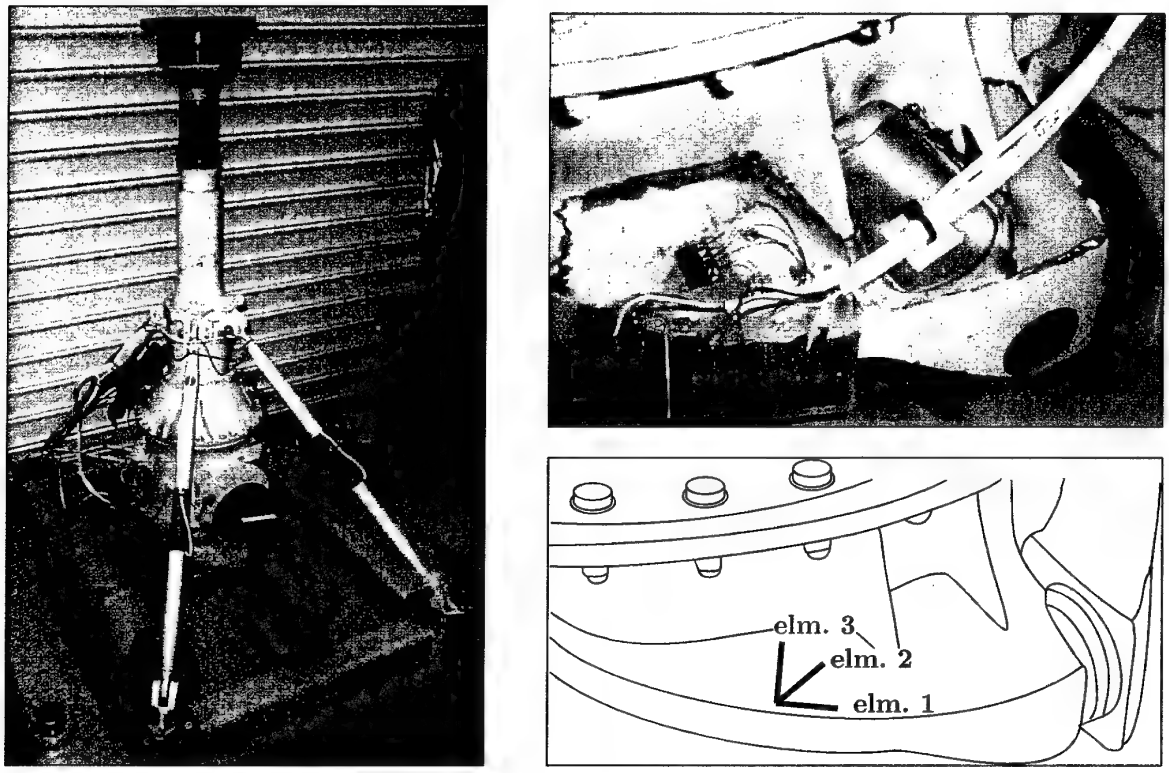

(i) (ii)

Figure 2.3: The (i) Squirrel gearbox and (ii) a close-up of the strain-gauge rosette. Part (ii) also shows the numbering of the elements within the strain gauge rosette.

- one rectangular, three-element rosette (Micro Measurements CEA-13-125UR-350) on the gear box housing, see Figure 2.3(ii).

In addition to these gauges, the force on all four load actuators (h_1, h_2, v_1, and v_2) and the output torque (Q) on the rotormast were also recorded.

Figure 2.1 shows the locations of the strain gauges on the gearbox. The two struts shown obscure a further two struts, and hence arrowhead pointers are used to highlight the two strain gauges on these obscured struts.

Figure 2.3 shows photographs of the Squirrel gearbox. Part (i) shows the back view of the complete gearbox with rotormast and struts attached. Part (ii) of this figure shows a close up of the gearbox with the active rosette bonded to the gearbox housing, and three dummy rosettes used for bridge completion on unstrained dummy plates. The element numbering and directional sense of the active rosette is shown as a schematic figure underneath this close-up photo.

A plot of the strain response (for the gearbox strain gauge rosette) against torque is

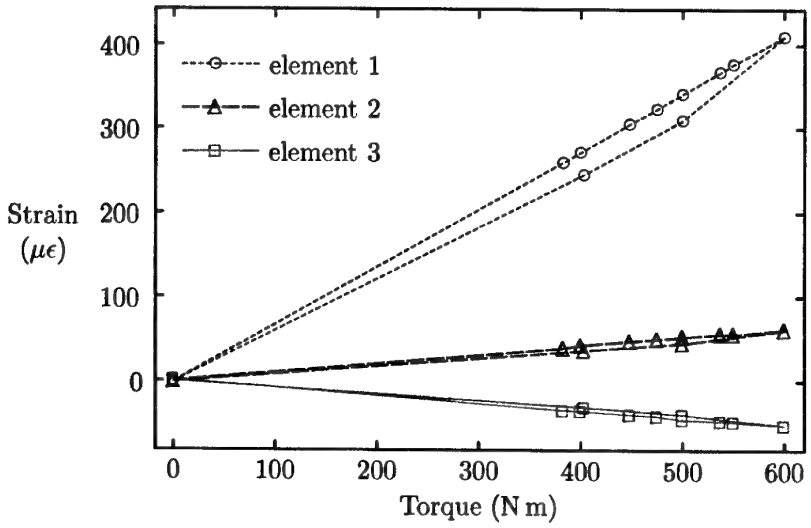

Figure 2.4: Response from gearbox strain gauge rosette. The response to the applied torque is given in microstrain.

shown in Figure 2.4. Using the biaxial stress equation [10] the maximum and minimum principal strains are

$$\epsilon_{\max,\min} = \frac{(\epsilon_1 + \epsilon_3)}{2} \pm \frac{\sqrt{(\epsilon_1 - \epsilon_2)^2 + (\epsilon_2 - \epsilon_3)^2}}{\sqrt{2}},$$

and the angle of the maximum strain from element 1 is

$$\alpha_{\max} = \frac{1}{2} \tan^{-1} \left(\frac{2\epsilon_2 - \epsilon_1 - \epsilon_3}{\epsilon_1 - \epsilon_3} \right),$$

where ϵ_i is the strain at the ith strain gauge element and if $\epsilon_1 < \epsilon_3$ then add $\pi/2$ to $\alpha_{\max}$. (The angles between elements 1 and 2 and elements 1 and 3 are respectively 45° and 90°, see Figure 2.3(ii).) At a 600 N m torque, the maximum and minimum principal stresses were 31 MPa and 3.6 MPa, respectively. The maximum principal strain, again at a 600 N m torque, was 440 $\mu\epsilon$ and occurs −13° from element 1 (the minimum strain was −81 $\mu\epsilon$).

Figure 2.5 shows photographs of the strain gauges on both a strut and the dog-bone. The strut picture, Figure 2.5(i), has an inset photograph showing the strain-gauged section of the strut enlarged. The main dog-bone picture, Figure 2.5(ii), shows the *top* of the dog-bone's strain-gauged section, while the inset photograph shows the *bottom* of this section. In the dog-bone photograph, the three sets of strain gauges (namely, horizontal bending, vertical bending, and tension-compression gauges) are labelled. The horizontal bending gauges, located on the left flange (as seen in the photograph) of the dog-bone's I-beam, are not clearly seen because of the angle of this photograph.

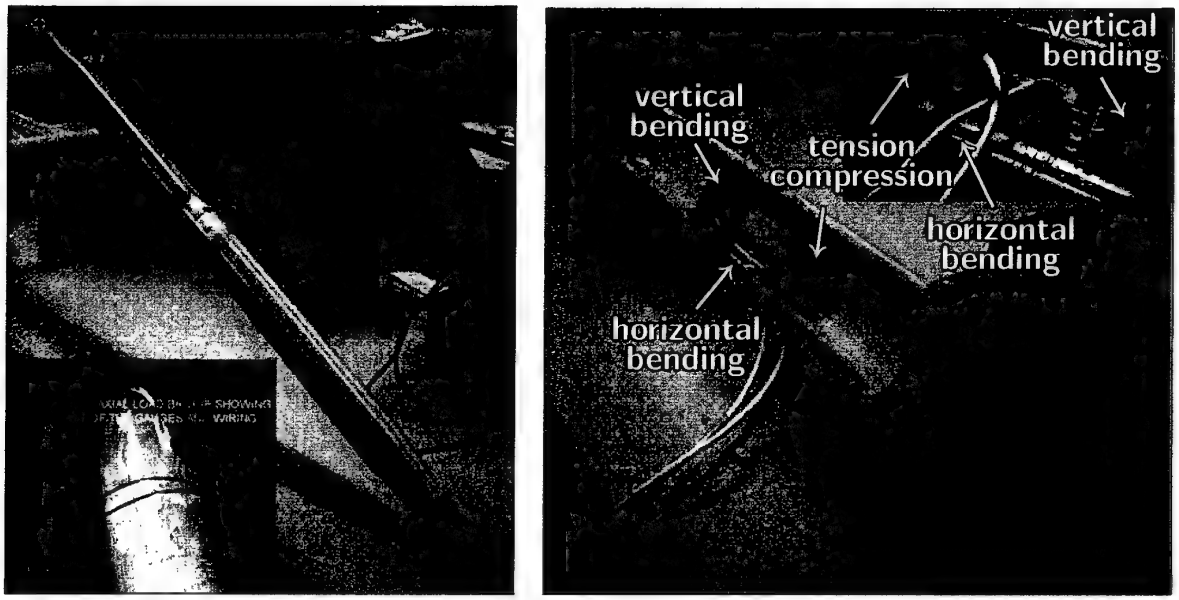

(i) (ii)

Figure 2.5: Photographs showing the strain gauges on both the (i) strut and (ii) dog-bone. The dog-bone photograph shows both the top (main photograph) and bottom (inset photograph) of the dog-bone.

3 Description of the Testing Program

Table 3.1 shows the operating limits for the Squirrel gearbox in the Helicopter Transmission Test Facility (HTTF). We used these operating conditions to determine sensible loading ranges for the testing program.[2]

Turbine	Rotor Load		
speed	**torque**	**vertical**	**horizontal**
6 000 rpm	+9 797 Nm	20 kN	2 kN

Table 3.1: The operating limits for the Helicopter Transmission Test Facility with the Squirrel gearbox fitted.

As input for the horizontal load, the HTTF required a magnitude h and an application angle θ. The inset box in Figure 2.1 shows the positive sense of the horizontal loading angle θ and the four loads h_1, h_2, v_1, and v_2. The horizontal loads h_1 and h_2 are obtained using the relations $h_1 = h\sin\theta$ and $h_2 = h\cos\theta$. The total vertical loading is $v = v_1 + v_2$, and for all the experimental load cases $v_1 = v_2$.

Before testing began, the HTTF was warmed up in three stages: (i) one minute at 2 000 N m and 1 000 rpm,[3] (ii) one minute at 4 000 N m and 2 000 rpm, and (iii) five minutes at 6 000 N m and 4 000 rpm. During these warm up stages no horizontal or vertical loads were applied.

After this seven minute warm up, the thirty-five loading cases (shown in Table 3.2) were each applied at 6 000 rpm for one minute. These loading cases were chosen so as to fill the parameter space—namely, vertical loading (v), horizontal loading (h and θ), and torque (Q)—as uniformly as possible. However, even three measurement points for each of these four parameters leads to eighty-one ($3^4 = 81$) load cases. In order to obtain a more manageable number of loading cases only the vertical load, one horizontal load (h_1), and torque were varied (the second horizontal load h_2 was held fixed at zero load) for the first twenty-seven cases. The last eight cases (cases 28–35) represent eight even angularly-spaced loads in the horizontal plane, that is, in the direction of the eight main compass points. (Note that load cases 27 and 28 are identical.)

After these thirty-five load cases the HTTF was warmed down, again in three stages with no horizontal or vertical loading: (i) one minute at 3 000 N m and 6 000 rpm, (ii) one minute at 1 000 N m and 4 000 rpm, and (iii) one minute at 0 N m and 1 000 rpm.

The original measurements taken were sampled (using the Metrum RSR512 recorder) at 625 samples per second (from a requested bandwidth of 78 Hz). The data were then resampled (via a digital-to-analogue and back-to-digital conversions) at 100 Hz, and finally down-sampled to the more manageable rate of 1 Hz.

[2]Additional operating restrictions were applied in order to avoid unnecessarily fast crack propagation within the gearbox. See Table 3.2 for the final loading set.

[3]Revolutions per minute of the turbine.

Case	Torque	Vertical	Horizontal	
	(N m)	(kN)	(kN)	θ
1	0	0	0	90°
2	0	0	0.9	90°
3	0	0	1.8	90°
4	0	9	0	90°
5	0	9	0.9	90°
6	0	9	1.8	90°
7	0	18	0	90°
8	0	18	0.9	90°
9	0	18	1.8	90°
10	2500	0	0	90°
11	2500	0	0.9	90°
12	2500	0	1.8	90°
13	2500	9	0	90°
14	2500	9	0.9	90°
15	2500	9	1.8	90°
16	2500	18	0	90°
17	2500	18	0.9	90°
continued on adjacent table...				

Case	Torque	Vertical	Horizontal	
	(N m)	(kN)	(kN)	θ
18	2500	18	1.8	90°
19	5000	0	0	90°
20	5000	0	0.9	90°
21	5000	0	1.8	90°
22	5000	9	0	90°
23	5000	9	0.9	90°
24	5000	9	1.8	90°
25	5000	18	0	90°
26	5000	18	0.9	90°
27	5000	18	1.8	90°
28	5000	18	1.8	90°
29	5000	18	1.7	315°
30	5000	18	1.8	0°
31	5000	18	1.7	45°
32	5000	18	1.8	90°
33	5000	18	1.7	135°
34	5000	18	1.8	180°
35	5000	18	1.7	225°

Table 3.2: The thirty-five load cases applied to the gearbox. The column labelled vertical load represents the total vertical load, that is, $v_1 + v_2$. The horizontal load is broken up into a magnitude and angle. All loading cases were applied at 6 000 rpm.

Only eight channels of data could be extracted at any one time from the data acquisition system. Thus to extract the fifteen recorded channels, the data were partitioned into two files, each file containing eight channels. Unfortunately, these partitioned measurements were not temporally aligned, that is, the files did not commence resampling at exactly the same position in time. In order to temporally re-align these partitioned measurements both files contained one common channel.

The re-alignment was calculated as follows. Let $\boldsymbol{x}^T = (x_1, x_2, \ldots, x_n)$ and $\widehat{\boldsymbol{x}}^T = (\widehat{x}_1, \widehat{x}_2, \ldots, \widehat{x}_n)$ denote vectors containing the common channel from the first and second files, respectively. To re-align these two vectors we want to minimise the error:

$$\mathrm{err}_m = \sqrt{\sum_{i=1}^{i=n-M} (x_{i-m\downarrow} - \widehat{x}_{i+m\uparrow})^2}, \tag{3.1}$$

where $m\downarrow = \min(0, m)$, $m\uparrow = \max(0, m)$, n is the number of elements in the vector $\boldsymbol{x}$, and M is the maximum lines to shift. Mathematically, $M = \max(-m_0, m_1)$, where $m_0 < 0$ and $m_1 > 0$ are the lower and upper bounds to try when re-aligning the common channel between the two files. Thus we want to find the number of line shifts m needed to minimises the error, that is,

$$\mathrm{err}_{\min} = \min_{m \in [m_0, m_1]} \mathrm{err}_m.$$

lines shifted	*truncated*	*comparison box*	*truncated*
$m = -2$	$x_{01}, x_{02},$	$x_{03}, x_{04}, x_{05}, x_{06}, x_{07}, x_{08}, x_{09}, x_{10}, x_{11}, x_{12}, x_{13},$	x_{14}
		$\widehat{x}_{01}, \widehat{x}_{02}, \widehat{x}_{03}, \widehat{x}_{04}, \widehat{x}_{05}, \widehat{x}_{06}, \widehat{x}_{07}, \widehat{x}_{08}, \widehat{x}_{09}, \widehat{x}_{10}, \widehat{x}_{11},$	$\widehat{x}_{12}, \widehat{x}_{13}, \widehat{x}_{14}$
$m = -1$	$x_{01},$	$x_{02}, x_{03}, x_{04}, x_{05}, x_{06}, x_{07}, x_{08}, x_{09}, x_{10}, x_{11}, x_{12},$	x_{13}, x_{14}
		$\widehat{x}_{01}, \widehat{x}_{02}, \widehat{x}_{03}, \widehat{x}_{04}, \widehat{x}_{05}, \widehat{x}_{06}, \widehat{x}_{07}, \widehat{x}_{08}, \widehat{x}_{09}, \widehat{x}_{10}, \widehat{x}_{11},$	$\widehat{x}_{12}, \widehat{x}_{13}, \widehat{x}_{14}$
$m = 0$		$x_{01}, x_{02}, x_{03}, x_{04}, x_{05}, x_{06}, x_{07}, x_{08}, x_{09}, x_{10}, x_{11},$	x_{12}, x_{13}, x_{14}
		$\widehat{x}_{01}, \widehat{x}_{02}, \widehat{x}_{03}, \widehat{x}_{04}, \widehat{x}_{05}, \widehat{x}_{06}, \widehat{x}_{07}, \widehat{x}_{08}, \widehat{x}_{09}, \widehat{x}_{10}, \widehat{x}_{11},$	$\widehat{x}_{12}, \widehat{x}_{13}, \widehat{x}_{14}$
$m = 1$		$x_{01}, x_{02}, x_{03}, x_{04}, x_{05}, x_{06}, x_{07}, x_{08}, x_{09}, x_{10}, x_{11},$	x_{12}, x_{13}, x_{14}
	$\widehat{x}_{01},$	$\widehat{x}_{02}, \widehat{x}_{03}, \widehat{x}_{04}, \widehat{x}_{05}, \widehat{x}_{06}, \widehat{x}_{07}, \widehat{x}_{08}, \widehat{x}_{09}, \widehat{x}_{10}, \widehat{x}_{11}, \widehat{x}_{12},$	$\widehat{x}_{13}, \widehat{x}_{14}$
$m = 2$		$x_{01}, x_{02}, x_{03}, x_{04}, x_{05}, x_{06}, x_{07}, x_{08}, x_{09}, x_{10}, x_{11},$	x_{12}, x_{13}, x_{14}
	$\widehat{x}_{01}, \widehat{x}_{02},$	$\widehat{x}_{03}, \widehat{x}_{04}, \widehat{x}_{05}, \widehat{x}_{06}, \widehat{x}_{07}, \widehat{x}_{08}, \widehat{x}_{09}, \widehat{x}_{10}, \widehat{x}_{11}, \widehat{x}_{12}, \widehat{x}_{13},$	$\widehat{x}_{14}$
$m = 3$		$x_{01}, x_{02}, x_{03}, x_{04}, x_{05}, x_{06}, x_{07}, x_{08}, x_{09}, x_{10}, x_{11},$	x_{12}, x_{13}, x_{14}
	$\widehat{x}_{01}, \widehat{x}_{02}, \widehat{x}_{03},$	$\widehat{x}_{04}, \widehat{x}_{05}, \widehat{x}_{06}, \widehat{x}_{07}, \widehat{x}_{08}, \widehat{x}_{09}, \widehat{x}_{10}, \widehat{x}_{11}, \widehat{x}_{12}, \widehat{x}_{13}, \widehat{x}_{14}$	

Figure 3.1: An example of the re-alignment algorithm with $m_0 = -2$, $m_1 = 3$, and $n = 14$. Only the data within the comparison box is used during re-alignment. The case with the minimum difference between the vectors $\boldsymbol{x}$ and $\widehat{\boldsymbol{x}}$ is the correct re-alignment point.

An example of this re-alignment algorithm is shown in Figure 3.1. Only the data bounded by the comparison box is used during the re-alignment process. All data lying outside the comparison box is discarded during re-alignment.

We now see that Equation (3.1) measures the distance between the two vectors $\boldsymbol{x}$ and $\widehat{\boldsymbol{x}}$ under the mth truncation. (Figure 3.1 shows how the mth truncation works, namely, data outside the comparison box is discarded.)

Due to the digital-to-analog and back-to-digital conversions and the resamplings, the channel used for the temporal re-alignment in the partitioned measurements was not identical in the two files (due to quantisation error and noise). Even at the optimal temporal re-alignment there was approximately a 7% relative difference between the same channel in the two files containing the partitioned measurements (see Figure 3.2). This 7% error is an order of magnitude larger than the error expected. Without a detailed analysis of the conversion systems it is impossible to determine where these additional conversion errors were introduced. Since the synthesis model verification is not affected by this resampling discrepancy, no further analysis of the conversion systems was undertaken.

The percentage relative error in Figure 3.2 was calculated as

$$\%\ \mathrm{err}_m = \frac{\mathrm{err}_m}{\mathrm{err}_{\|m\|}} \times 100,$$

where $\mathrm{err}_{\|m\|}$ is the length of the averaged vectors $\boldsymbol{x}$ and $\widehat{\boldsymbol{x}}$ (under the mth truncation),

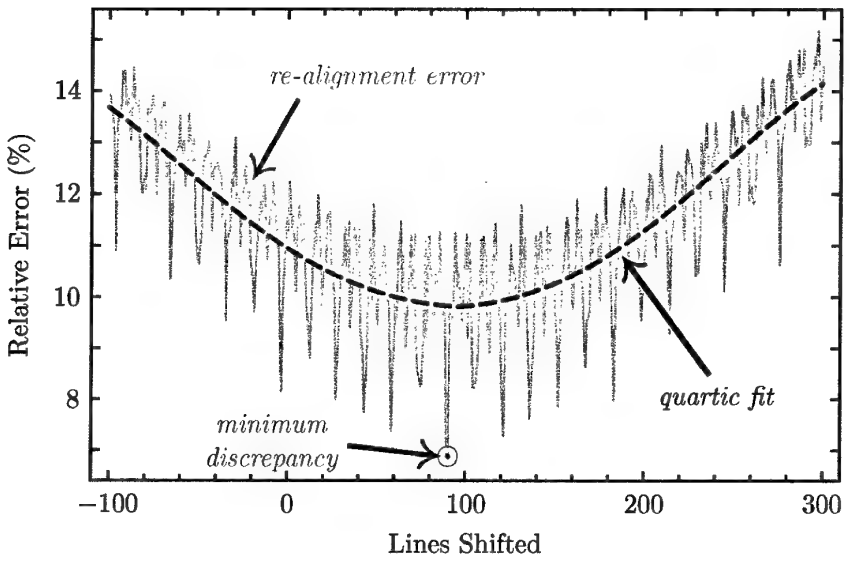

Figure 3.2: Temporally re-aligning partitioned files. The solid light green curve denotes the normalised error when the partitioned files are shifted with respect to each other. The broken black curve is the quartic fit to the solid light green curve. The symbol "⊙" shows where the minimum normalised error occurs, that is, where the optimum re-alignment occurs.

that is,

$$\mathrm{err}_{\|m\|} = \sqrt{\sum_{i=1}^{i=n-M} \left(\frac{x_{i-m\downarrow} + \widehat{x}_{i+m\uparrow}}{2} \right)^2}. \tag{3.2}$$

Note the similarity between err_m given by Equation (3.1) and $\mathrm{err}_{\|m\|}$ given by Equation (3.2). Both equations measure the length of a vector, either the difference or the average of the two vectors $\boldsymbol{x}$ and $\widehat{\boldsymbol{x}}$ (under the mth truncation).

The quartic fit in Figure 3.2 shows that there is a general trend between the relative error and the lines shifted leading to a minimum. However, it is unsettling to see such large variations (approximately a 5% fluctuation) between adjacent line shifts, especially when this variation should only be due to the two resamplings.

Figure 3.3 shows a portion of the Horizontal Force 1 data, which was used to calculate the file re-alignment. (See Figure 3.4 for a plot of the complete Horizontal Force 1 data.) The optimum re-alignment, as depicted in Figure 3.2, was used in this Horizontal Force 1 plot. In Figure 3.3 there are 13 000 samples (from 100 Hz data), which represents approximately two minutes worth of data. Within this plot there are two zoomed sections, each shows 75 samples and represents approximately 0.75 seconds of data. Both in the main plot and zoomed sections, the two time history lines closely follow each other demonstrating a good re-alignment between the two files. As can be seen in the first minute of this plot there appears to be a voltage drift between the two resamplings of the same data channel. This voltage drift diminishes for the remaining time shown.

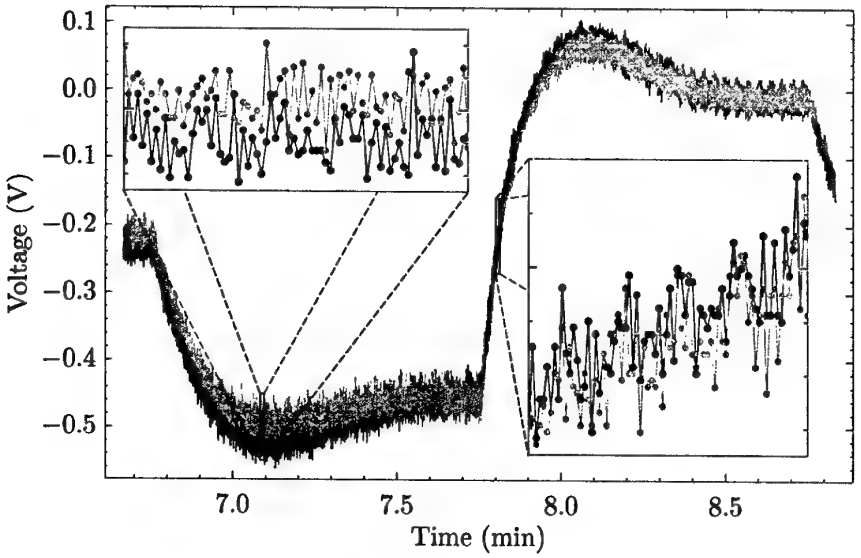

Figure 3.3: Time history sample of the file re-alignment using the 100 Hz data from the Horizontal Force 1 gauge. Both the main plot and zoomed sections show that the files are well aligned. The first minute of this plot shows the drift in resampling the same channel.

The data recorded by the Metrum were all voltage readings. The following factors should be used to convert from voltage to the appropriate engineering units.

- Converting strain gauge readings from voltage to strain: 2 500 $\mu\epsilon$/V.
- Converting rotor toque (Q) readings from voltage to Newton metres: -1300 N m/V.
- Converting vertical force (v_1 and v_2) readings from voltage to Newtons: -2050 N/V.
- Converting horizontal force (h_1 and h_2) readings from voltage to Newtons: -450 N/V.

Time history plots of the raw measurements (in volts) are shown in Figure 3.4. In each plot, the horizontal axis represents time (approximately 41 minutes is shown). The length of the vertical scale bar ▮ represents 0.1 V (except in the plot entitled "Vertical Bending", where the length of the scale bar ▮ represents 0.05 V).

In Figure 3.4 the raw data are represented by the light blue curves. For easier visualisation this raw data was smoothed using a Savitzky-Golay smoothing filter (see Press et al. [9]) and is depicted in the plots as the black curve. The smoothing was performed using an 11-point moving window (essentially a convolution), that is,

$$g_i = \sum_{j=-5}^{5} c_j f_{(i+j)} \qquad \text{for } i = 1, \ldots, n, \tag{3.3}$$

where f and g represent the raw and smoothed data, respectively, and n is the number of raw measurements taken. The smoothing operation given by Equation (3.3) is equivalent

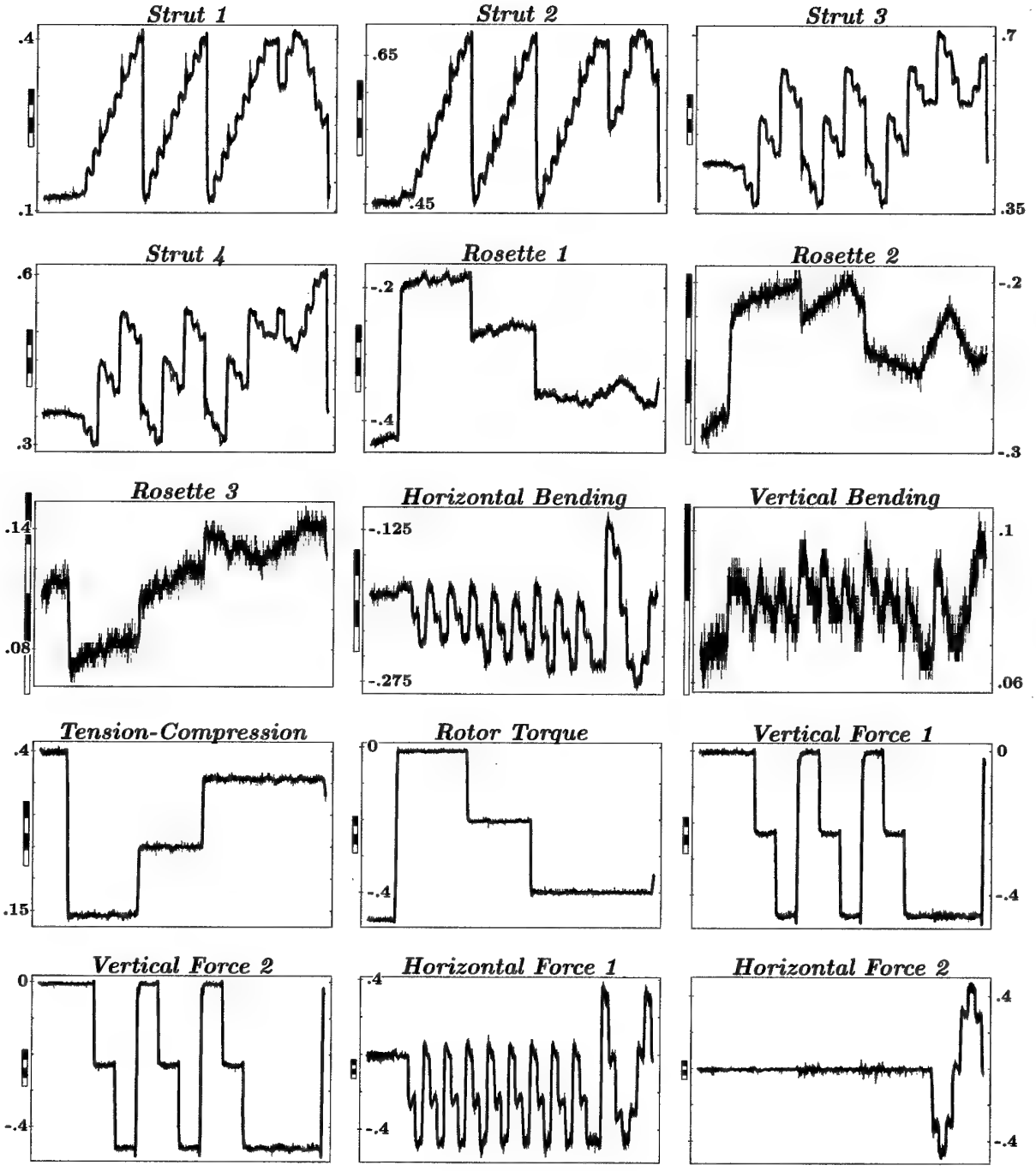

Figure 3.4: Time history plots of the raw voltage measurements. The length of the vertical scale bar ▮ (to the left of each plot) represents 0.1 V *(except in the plot entitled "Vertical Bending", where the length of the scale bar ▮ represents* 0.05 V*).*

to applying a least-squares quadratic fit to the eleven points surrounding and including the point of interest. Press et al. [9] give the following values for c_j:

$$(c_0, c_1, c_2, c_3, c_4, c_5) = (0.207, 0.196, 0.161, 0.103, 0.021, -0.084)$$

and $c_{-j} = c_j$ for $j = 1, 2, \ldots, 5$.

The black curves in Figure 3.4 (which represent the smoothed results) were obtained by recursively applying the smoothing operation five times. Further applications of this smoothing operator began to erase what were thought to be key features of the loading. On the other hand, too few applications of this smoothing operator did not reduce the "noise" sufficiently. By "noise" we mean both spurious loads (due to electrical measurement errors) and mechanical loads (due to gearbox vibration) not experienced by the rotormast head. Thus the number of smoothing operator applications, five, was chosen through trial and error to satisfy conflicting requirements—namely, reducing noise while retaining key loading features.

Mathematically, let $\boldsymbol{g}_0 = \boldsymbol{f}$, $\boldsymbol{g}_1 = \boldsymbol{g}$, and $\mathcal{S}$ represent the smoothing operation. Using this notation Equation (3.3) may be rewritten as $\boldsymbol{g}_1 = \mathcal{S}(\boldsymbol{g}_0)$, and the black curves represents $\boldsymbol{g}_5$, where $\boldsymbol{g}_k = \mathcal{S}(\boldsymbol{g}_{k-1})$ for $k = 1, 2, \ldots, 5$.

So that the length of the smoothed data vector $\boldsymbol{g}$ was the same as the length of the measured data vector $\boldsymbol{f}$, the original raw measurement vector was padded. Five additional copies of both the values f_1 and f_n were added on the left- and right-hand sides of $\boldsymbol{f}$, respectively. Mathematically, $f_i = f_1$ for $i = -4, -3, \ldots, 0$ (the left-hand side) and $f_i = f_n$ for $i = n+1, n+2, \ldots, n+5$ (the right-hand side), so that the padded vector contained $n + 10$ elements before smoothing and n elements after smoothing.

The smoothed data was only used for the plots shown in Figure 3.4, the raw data was used for all the calculations that follow. The smoothed results give us an indication of the level of noise present in the measurements.

4 Results

In this section we compare and contrast the loads-synthesis results from the least squares (LS) and instrumental variable (IV) models. For brevity, within this section the ten input and five output parameters will be referred to by a number code instead of name (see Table 4.1 for the numbering code). Thus, for example, the combination of input parameters $\{1, 3, 5, 6, 9\}$ would denote the combination of gauges located on Struts 1 and 3, Rosettes 1 and 2, and the Vertical Bending gauge on the dog-bone.

	Input parameters		Output parameters
(1)	Strut 1	(1)	Rotor torque
(2)	Strut 2	(2)	Vertical force 1
(3)	Strut 3	(3)	Vertical force 2
(4)	Strut 4	(4)	Horizontal force 1
(5)	Rosette 1	(5)	Horizontal force 2
(6)	Rosette 2		
(7)	Rosette 3		
(8)	Horizontal bending		
(9)	Vertical bending		
(10)	Tension-compression		

Table 4.1: The numbering code used for the input and output parameters.

The errors in this section are calculated using the two-norm. The square of the two-norm is given by $\|\boldsymbol{x}\|_2^2 = \sum_{i=1}^{n} x_i^2$, where $\boldsymbol{x}$ is the vector $(x_1, x_2, \ldots, x_n)$. The errors were normalised by the measured results, thus the normalised two-norm error used in this section is given by

$$\text{error} = \frac{\|\boldsymbol{y}_s - \boldsymbol{y}_m\|_2}{\|\boldsymbol{y}_m\|_2}, \tag{4.1}$$

where $\boldsymbol{y}_s$ and $\boldsymbol{y}_m$ denote vectors containing the synthesised and measured results, respectively.

There were ten input parameters available to synthesise the five output parameters. We theoretically require only five input parameters to synthesise the five output parameters.[4] Choosing five input parameters from the ten input parameters available means there are $C_5^{10} = 252$ different combinations of input parameters available to synthesise the five output parameters.

Figure 4.1 shows two examples (best and worst synthesis) of the rotor loads-synthesis techniques. The IV, LS, and measured (meas) results are shown respectively as light blue, medium green, and dark red lines.

The five large plots in this figure show the best performing synthesis results. The combination of input parameters $\{1, 2, 3, 4, 10\}$ led to this best synthesis result. It was

[4]More precisely, only five input parameters are required if they are linearly independent and they span the space of the five output parameters.

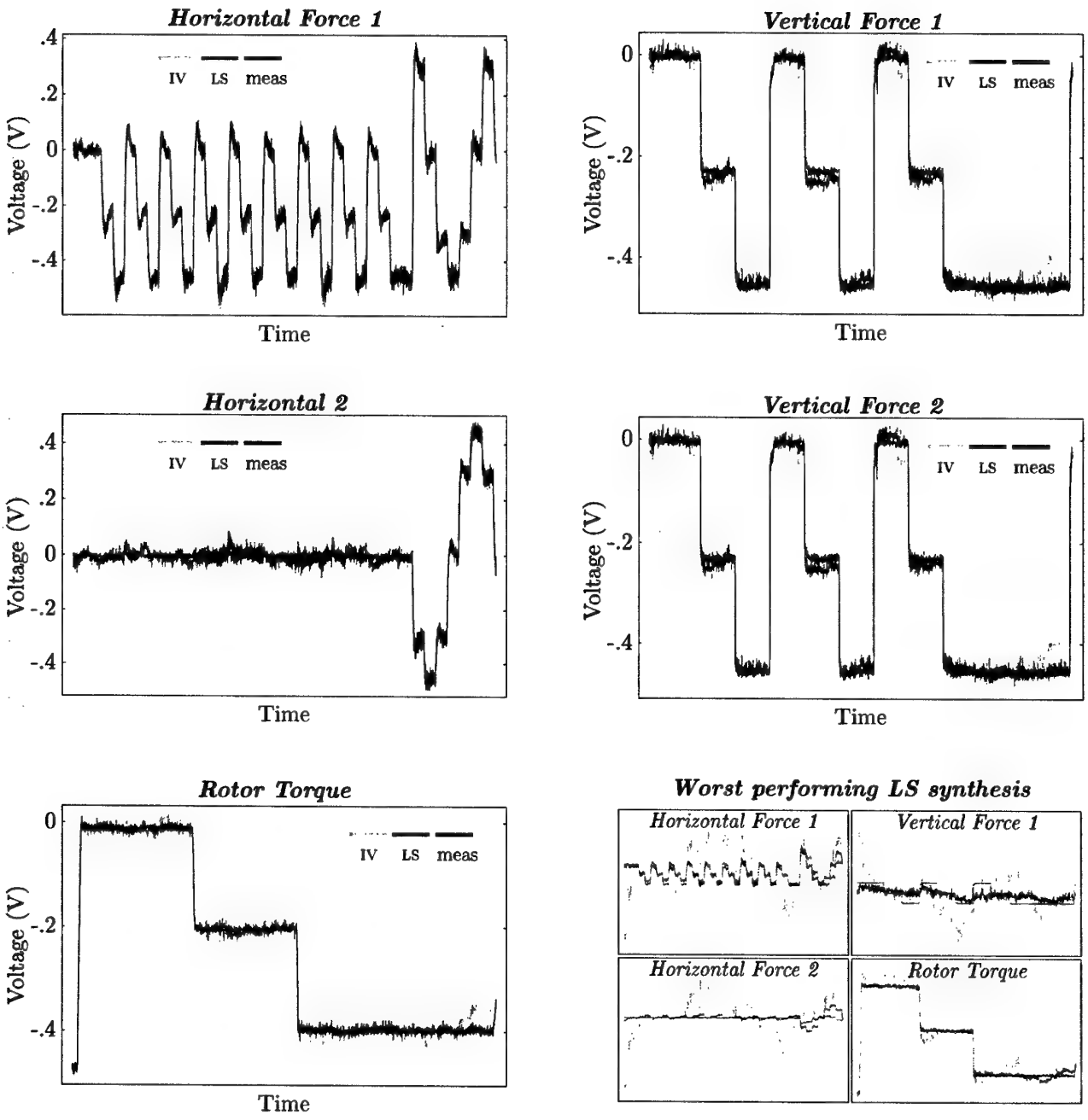

Figure 4.1: Plots showing the best performing instrumental variable (IV) and least squares (LS) loads synthesises of the measured (meas) parameters. The set of four plots in bottom right-hand panel show the worst performing LS load synthesis.

coincidental that this combination of input parameters led to both the best LS and the best IV solutions. Because there were five output parameters to be synthesised, the "best" result was calculated as the input parameter combination that returned the smallest two-norm error. In other words, if e_i represents the normalised two-norm error from the ith output parameter, than the "best" combination of input parameters is the one that minimises $\|\boldsymbol{e}\|_2$, where $\boldsymbol{e}$ is the vector $(e_1, e_2, \ldots, e_5)$. A similar definition holds for the "worst" synthesis result; namely, the combination of input parameters that maximises $\|\boldsymbol{e}\|_2$.

The bottom right-hand panel of four plots in Figure 4.1 shows the worst synthesis result from the LS model. The combination of input parameters $\{6, 7, 8, 9, 10\}$ led to this worst LS synthesis result. For clarity within this panel, the synthesis history of the output parameter Vertical Force 2 (which is similar to the result for Vertical Force 1) is not shown in this worst performing panel.

The combination of input parameters $\{3, 5, 6, 7, 10\}$ led to the worst IV synthesis result, which was over 100 times larger than the worst LS result.

Table 4.2 shows the normalised error, as defined in Equation (4.1), for the best and worst performing LS and IV synthesis results. The errors from the best performing IV and LS cases are comparable, more specifically, the IV errors are approximately one-and-a-half times larger than the LS errors. For the worst performing cases, however, the IV error ranges from 70 to 200 times larger than the associated worst LS error.

Output	**Best performing**		**Worst performing**	
parameter	**LS error**	**IV error**	**LS error**	**IV error**
(1) Rotor torque	0.030	0.051	0.030	2.2
(2) Vertical force 1	0.044	0.070	0.23	45
(3) Vertical force 2	0.043	0.070	0.23	45
(4) Horizontal force 1	0.070	0.089	0.62	120
(5) Horizontal force 2	0.15	0.17	0.75	61

Table 4.2: Normalised error for the worst and best performing least squares (LS) and instrumental variables (IV) synthesis results.

Trouble can be expected in the numerical solution of the least squares method whenever the condition number of the least squares matrix is large. According to Golub and Van Loan [3, § 5.3.5], this trouble occurs when $\kappa_2(A) \approx 1/u$, where κ_2 is the two-norm condition number [3, § 2.7.2], A is the least squares matrix, and u is the machine's unit roundoff. As a rule of thumb, the logarithm (base 10) of the condition number gives the number of significant digits lost due to round-off error, that is,

$$\text{digits lost to round-off} \approx \log_{10}(\kappa_2). \tag{4.2}$$

Before continuing further, it will prove useful to summarise some of the main linear algebra results we will need. Although it is not exactly the way to determine the LS or

IV models, it will prove useful to look at a simple analogy. Consider a linear single-input single-output (SISO) system, which we approximate by $y = ax$. Here x is the input parameter, y is the output parameter, and a is the coefficient relating the input parameter to the output parameter. Let us consider m measurements of this SISO system using this simple linear model:

$$\boldsymbol{y} = \boldsymbol{x}a. \tag{4.3}$$

The vector $\boldsymbol{x} \in \mathbb{R}^m$ denotes m measurements of the input parameter x, while the vector $\boldsymbol{y} \in \mathbb{R}^m$ denotes m measurements of the output parameter y. Using calibration data we know $\boldsymbol{x}$ and $\boldsymbol{y}$ and so can determine the coefficient a using the relation $a = (\boldsymbol{x}^T\boldsymbol{y})/(\boldsymbol{x}^T\boldsymbol{x})$. Once the calibration is complete, given some input $\boldsymbol{x}$ we can synthesise the output $\boldsymbol{y}$ using the coefficient a and Equation 4.3.

We can generalise this analogy to a multiple-input single-output (MISO) system, with n input variables, which we model by $y = a_1x_1 + \cdots + a_nx_n$. Let us consider m measurements of this MISO system using this simple linear model:

$$\boldsymbol{y} = \boldsymbol{X}\boldsymbol{a}, \tag{4.4}$$

where the vector $\boldsymbol{y} \in \mathbb{R}^m$ contains m measurements of the output parameter y, the matrix $\boldsymbol{X} \in \mathbb{R}^{m \times n}$ contains m measurements of the n input parameters x_i (for $i = 1, \ldots, n$), and the vector $\boldsymbol{a} \in \mathbb{R}^n$ contains one coefficient for each x_i (that is, n coefficients). If $\boldsymbol{X}^{-1}$ is the inverse of the matrix $\boldsymbol{X}$, then solving for the coefficient vector $\boldsymbol{a}$ we have that

$$\boldsymbol{a} = \boldsymbol{X}^{-1}\boldsymbol{y}. \tag{4.5}$$

There are two main problems in determining the coefficient vector $\boldsymbol{a}$:

- Ill-conditioning (that is, collinearity) of the matrix $\boldsymbol{X}$ causes small errors in $\boldsymbol{y}$ to induce large errors in the solution of $\boldsymbol{a}$ (see Equation 4.5).
- Solving Equation 4.5 for the coefficient vector $\boldsymbol{a}$ with errors in both $\boldsymbol{X}$ and $\boldsymbol{y}$, due to noise, may lead to large errors.

The first of these problems is by far the more serious, since (provided the noise is unbiased) errors due to noise can be reduced by using additional measurements.

It will prove useful to keep this simple MISO system analogy in mind when, in solving for the LS or IV models, we refer to either ill-conditioning or noise.

As would be expected, the five output parameters were synthesised with varying degrees of success by the different input-parameter combinations. Figure 4.2 compares how well the two techniques (LS and IV) performed in synthesising the output parameters. This figure shows plots of the ratio of errors (instrumental variable error to least square error) for the different combinations of input parameters. These error ratios are plotted against the condition number of the matrix containing the data from the input parameters. The scale to the right of each plot maps colour to LS error. All of the scales (vertical, horizontal, and colour) on these plots are logarithmic.

These error ratios clearly demonstrate that—in general—the LS model more accurately synthesises load than does the IV model. An earlier report [8] demonstrated that the IV

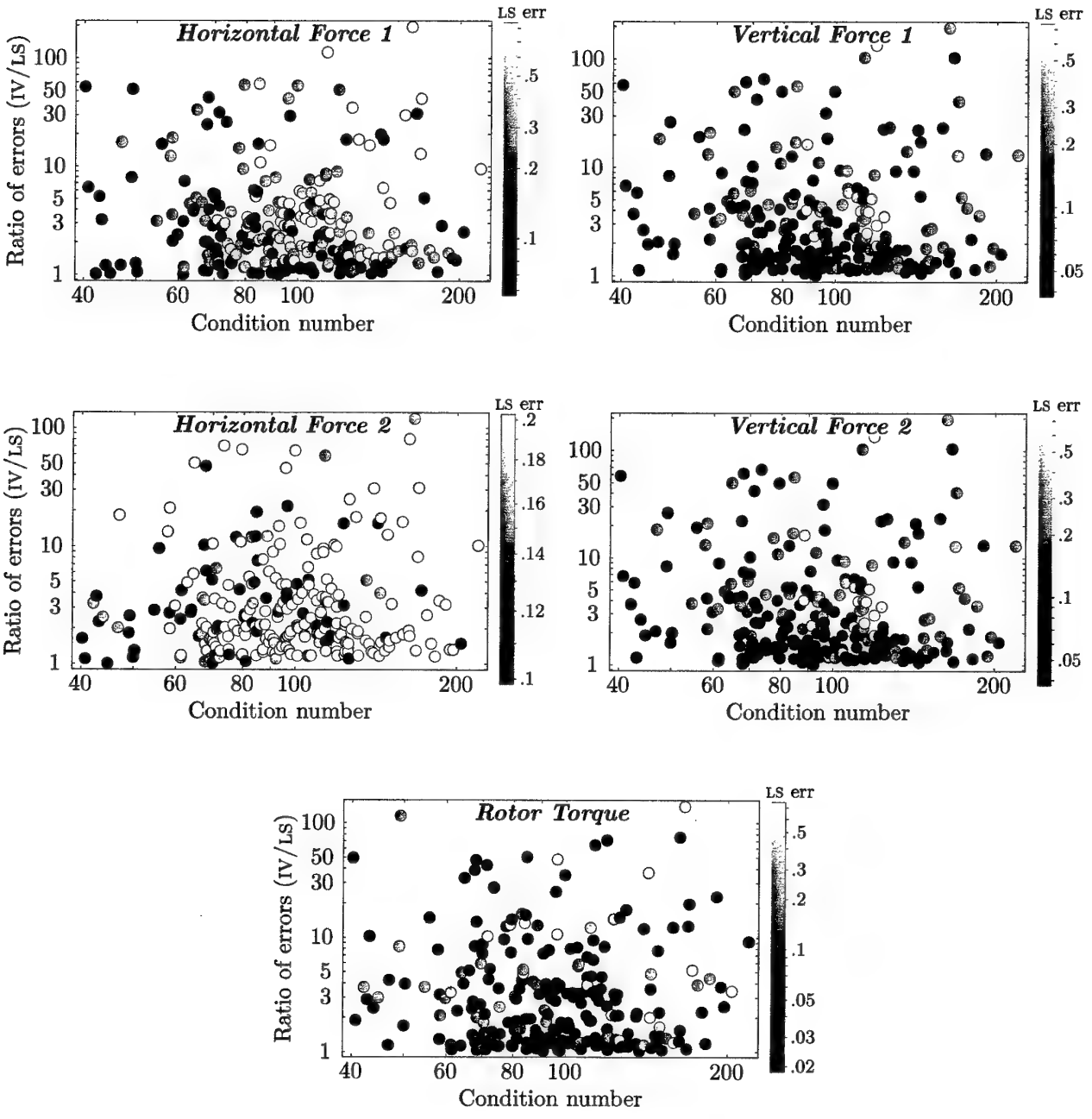

Figure 4.2: Plots showing the ratio of instrumental variable (IV) error to least squares (LS) error versus condition number. The shaded scale (to the right of each plot) pairs a dot's shading with its LS error. All scales are logarithmic.

model would outperform the LS model *only* when the condition number (of the system to be solved) was large and there was significant noise. The condition number in the current experimental results is relatively small—approximately 100. Thus according to Equation (4.2), the LS synthesis would be losing approximately two digits of accuracy from the sixteen digits available under normal single-precision arithmetics. The noise level in the measurements also appeared to be low. For example, in Figure 3.4 compare the smoothed measurements (in black) with the raw measurement (in light blue), the difference between these two curves gives an indication of the noise.

The plots in Figure 4.2 also demonstrate the loads-synthesis effect of increasing condition number. Generally, and as expected, the points to the left of these plots are darker (that is, have lower synthesis errors) than the points to the right. However, this correlation between condition number and loads-synthesis error is only weakly demonstrated in these plots due to the small range of condition numbers.

Given that the LS model seemed to perform better for this gearbox experimental data, the effect of varying the number of input parameters on the error from the LS model was investigated. Figure 4.3 shows plots of how the LS error varies with both condition number and the number of input parameters used in loads synthesis. A plot of the output parameter Vertical Force 2 (which is similar to the result for Vertical Force 1) is not shown. In these plots, the LS error is depicted in three-dimensions and these error points are projected onto the plot's three perpendicular planes. The colours denote the number of inputs.

We see several expected phenomena in Figure 4.3. The condition number increases as the number of inputs (used in the synthesis model) increases. Moreover, for the now known to be well-conditioned system: The synthesis results improve with additional inputs. And the best result for all output parameters is obtained when all ten input parameters are used in the loads synthesis.

Unexpectedly, the synthesis error decreases with increasing condition number, which is the opposite effect to that which was expected. This unexpected behaviour may be due to the small range of condition numbers found when using different input combinations. (In other words, using Equation 4.2 we are only losing two digits accuracy in the matrix inversion.) Alternatively, the additional information provided by the extra gauges may more than compensate for the increased collinearity between gauges.

Figure 4.4 shows the statistical distribution of normalised error when different combinations of input parameters are used to synthesise the output parameters. These error distributions are plotted against the number of input parameters used in the loads-synthesis model.

The distributions of errors for the LS model are depicted by the blue shaded regions. The lower and upper bounds of the light blue region give the minimum and maximum, respectively. The first and third quartiles[5] are respectively depicted by the lower and upper bounds of the mid-blue region. The central dark blue line denotes the distribution's median (that is, second quartile).

[5]By definition, 25% of the data have values below the first quartile and 75% have values below the third quartile.

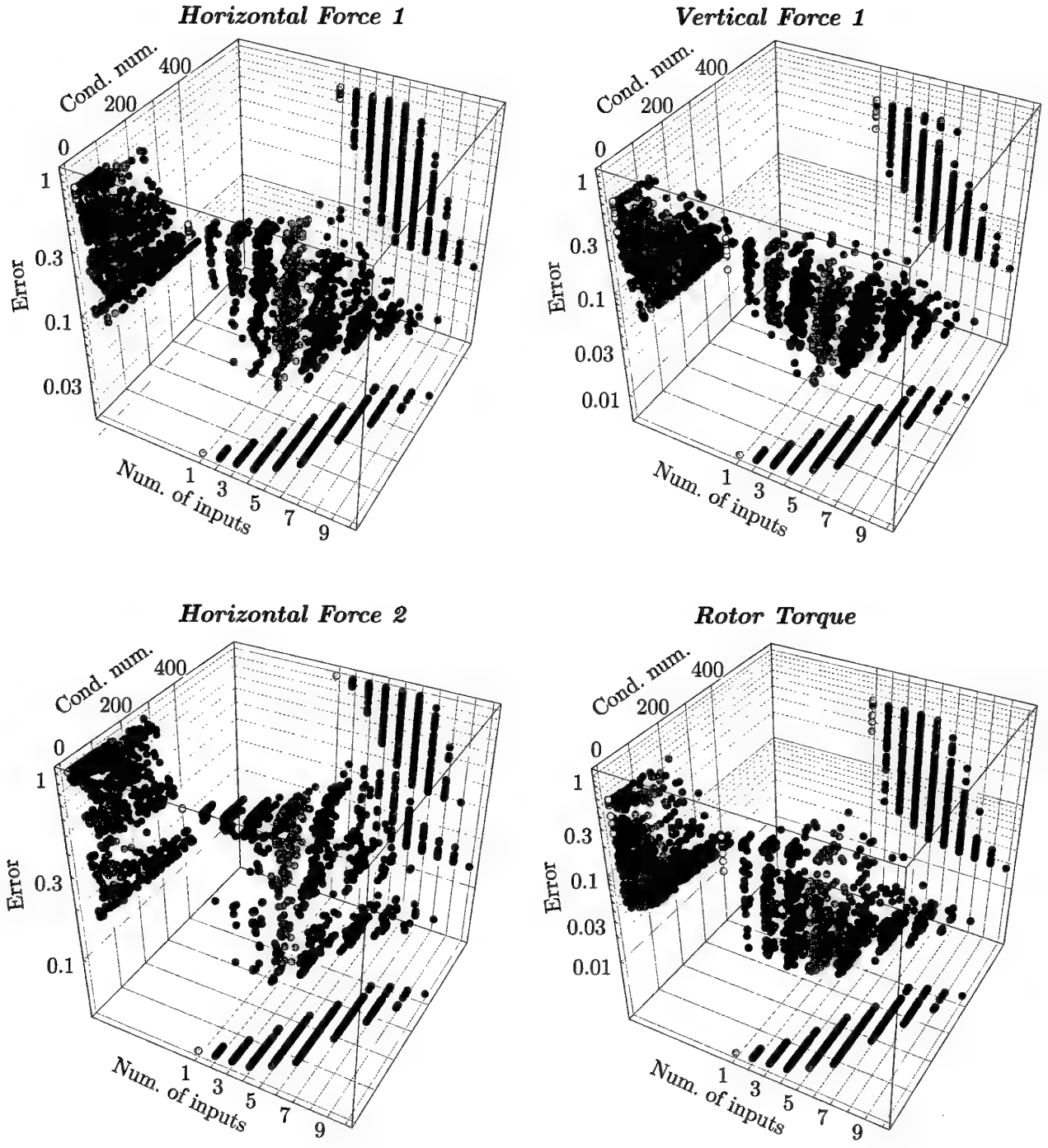

Figure 4.3: Error (of four output parameters) for the least squares (LS) loads synthesis of the measured parameters. This error is plotted against the number of input parameters (Num. of inputs) and the condition number (Cond. num.) of the LS matrix. The colours correspond to the number of inputs.

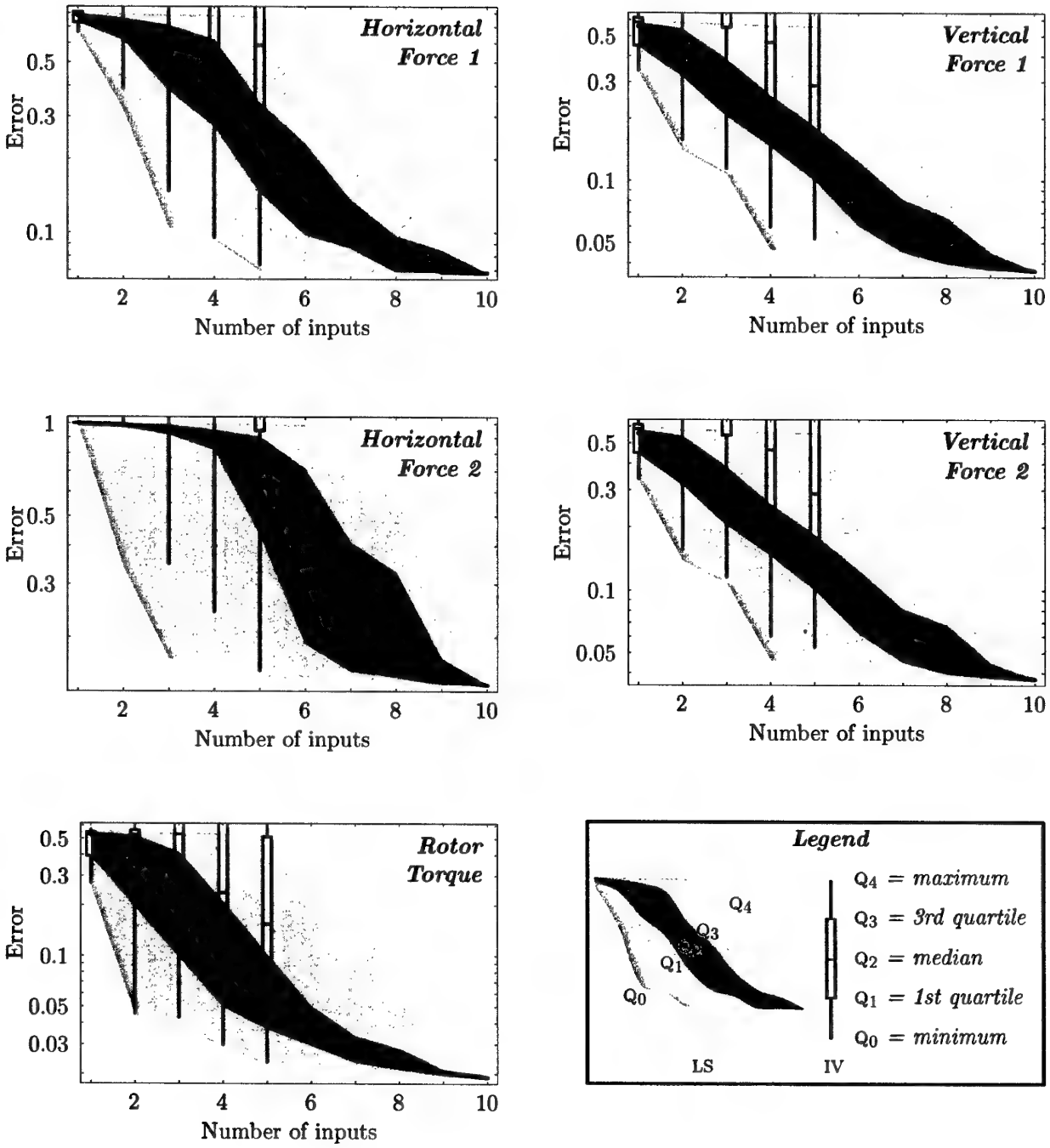

Figure 4.4: Plots showing the statistical distribution of normalised error versus the number of input parameters used in the loads-synthesis model. The distributions were generated using all the different input-parameter combinations for a fixed number of inputs. The blue shaded regions and box-and-whiskers plots respectively depict error distributions from the least squares (LS) and instrumental variable (IV) models.

There is only one combination of 10 inputs, that is, $C_{10}^{10} = 1$. So strictly speaking the statistical distributions shown in Figure 4.4 for the cases of 10 input parameters is depicted only for the continuity of the plots. It is impossible to determine the first and third quartiles of a single value; and the minimum, median, and maximum of a single value makes little sense.

The distributions of errors for the IV model are depicted by the box-and-whiskers plots. The lower and upper ends of the whisker lines give the minimum and maximum, respectively. The lower and upper bounds of the box respectively depict the first and third quartiles. The horizontal line inside the box depicts the median. Due to implementation limitations of the IV model, only the case of five input parameters or less are depicted in these IV error box plots. As a limitation, Johnston and DiNardo [4] state that to implement the IV technique, the number of instrumental variables has to be at least as large as the number of input variables. We have used the same number of input and instrumental variables in the IV models.

As can be seen in Figure 4.4, the median error decreases exponentially with increasing number of inputs. For the Horizontal Force 2 load, this exponential decrease in median error does not occur until there are at least five inputs. This late error decrease is probably due to the fact that for most of the testing the loading from the Horizontal Force 2 actuator is zero (see Figure 3.4).

Provided we choose the best combination of inputs, five inputs are enough to accurately synthesis the five output loads shown in Figure 4.4. There is only a marginal increase in synthesis accuracy between the best five-input model and the ten-input model. For any particular output parameter, the relative error between the best five-input model and the associated ten-input model varies between 2% and 16%.

From the LS and IV results in Figure 4.4 we see that the minimum of both models was comparable (except for Horizontal Force 2, where the errors for the 2, 3, and 4 input IV model were twice that of the corresponding LS model). However, the spread of the IV errors was considerably larger than the corresponding LS errors. As noted earlier for the five input case (see Figure 4.2), the worst IV error can be more than 100 times larger than the worst LS result. The IV model is very sensitive to the gauge combination chosen to perform the loads synthesis.

Artificially adding noise to the measurements produced similar results and slightly improved the condition number of the system to be solved! The added noise made the system appear even more orthogonal than it really was, resulting in an improved condition number.

5 Conclusion

The main aim of this experiment on the Squirrel gearbox was to validate the loads-synthesis model under challenging conditions—namely, using noisy measurements and collinear (that is, almost linearly dependent) gearbox gauges. We anticipate that gauges mounted on a real helicopter would experience these challenging conditions, and so we were attempting to simulate these conditions in this experiment.

Unfortunately, the chosen geometry of the gearbox gauges resulted in a set of equations that were linearly independent (in fact, they were almost orthogonal). This orthogonality meant that both techniques under investigation were able to easily synthesise the required loads.

Choosing a gauge geometry that results in either linear dependence or independence would probably be difficult on a complex structure like a helicopter. The best and simplest way to choose the gauge geometry would be to use existing data from a flight loads program (such as the joint ADF-USAF Black Hawk flight loads survey [2]). Different gauge combinations could then be easily and quickly tested for linear independence and noise in synthesising each required component load.

Alternatively, the fact that we obtained an almost orthogonal set of gauges (when we were trying to produce an almost linearly dependent set) may portend good news. Perhaps the selection of gauge locations on a real helicopter may not be as formidable as we envisaged? That is, most sets of gauge locations result in orthogonal systems, so that a simple load-synthesis technique would be sufficient to provide accurate results.

Only further experimental validation will determine which of these two scenarios is correct.

The level of noise-to-signal ratio was low for all gauges; in fact, most gauges had noise levels lower than 2%. From a testing perspective these low noise levels were less of a problem than the gauge orthogonality because noise could easily be added to the raw signals. Ironically, adding more noise (to this particular system) only improved the system's gauge orthogonality! Adding independent Gaussian noise to the raw gauge signals made the system appear even more orthogonal, probably because this independent noise further reduced the collinearity between different gauges.

In previous simulation work [8] we found that the instrumental variables (IV) model was better than the least squares (LS) model *only* when there were high noise levels in the measurements and the gauges were almost linearly dependent. When these two conditions were not present, both models produced comparable results. The experimental results obtained from the gearbox confirmed these previous simulation results, and demonstrated that the IV model errors were very sensitive to gauge combination. Choosing the wrong gauge combination for the IV model led to errors that were more than 100 times larger than the error produced by the best IV model. In contrast, the LS model was less sensitive to gauge combination, where the errors from the worst gauge combination were approximately 10 times larger than the errors found with the best gauge combination.

The next validation test of the IV synthesis model will be a blind test using data from the Black Hawk flight loads survey [2].

Acknowledgements

We would like to thank Mr Kenneth Vaughan for aiding in the testing program. The low noise levels achieved in this gearbox experiment were due to his expertise in all things experimental.

References

1. AEROSPATIALE, *Instruction Manual AS 350 [Squirrel], Rev. A*, January 1986.

2. R. BOYKETT AND C. FEALY, *Testing 'down-under': lessons learned on Black Hawk flight loads survey*, in Proceedings of the American Helicopter Society's 57th Annual Forum, Washington, DC, May 2001.

3. G. H. GOLUB AND C. V. VAN LOAN, *Matrix Computations*, Johns Hopkins, 2nd edn, 1989.

4. J. JOHNSTON AND J. DINARDO, *Econometric Methods*, McGraw-Hill, 4th edn, 1997. (See, in particular, § 5.5 "Instrumental Variables Estimators".)

5. D. C. LOMBARDO, *Helicopter structures—a review of loads, fatigue design techniques and usage monitoring*, Tech. Report 15, AR-00-137, Defence Science and Technology Organisation (Melbourne, Australia), May 1993.

6. F. G. POLANCO, *Estimation of structural component loads in helicopters: a review of current methodologies*, Tech. Report DSTO-TN-0239, Defence Science and Technology Organisation (Melbourne, Australia), December 1999.
(`http://www.dsto.defence.gov.au/corporate/reports/DSTO-TN-0239.pdf`)

7. F. G. POLANCO, *Development of a stress transfer function for an idealised helicopter structure*, Tech. Report DSTO-RR-0171, Defence Science and Technology Organisation (Melbourne, Australia), March 2000.
(`http://www.dsto.defence.gov.au/corporate/reports/DSTO-TN-0171.pdf`)

8. F. G. POLANCO, *Effects of noise on almost collinear systems*, Tech. Report DSTO-RR-0204, Defence Science and Technology Organisation (Melbourne, Australia), March 2001.
(`http://www.dsto.defence.gov.au/corporate/reports/DSTO-TN-0204.pdf`)

9. W. H. PRESS, S. A. TEUKOLSKY, W. T. VETTERLING, AND B. P. FLANNERY, *Numerical Recipes in C: the art of scientific computing*, Cambridge, 2nd edn, 1992. (See § 14.8 "Savitzky-Golay Smoothing Filters", pp. 650–655.)

10. W. C. YOUNG, *Roark's Formulas for Stress and Strain*, McGraw-Hill, 6th edn, 1989. (Biaxial stress: p. 88, Table 2, Condition 2.)

DISTRIBUTION LIST

Experimental Verification of Helicopter-Rotor Loads-Synthesis Models

Frank G. Polanco, Chris G. Knight, Scott A. Dutton, and Phil Ferrarotto

	Number of Copies
AUSTRALIA	
DEFENCE ORGANISATION	
S & T Program	
Chief Defence Scientist FAS Science Policy AS Science Corporate Management Director General Science Policy Development	1
Counsellor Defence Science, London	Doc Data Sht
Counsellor Defence Science, Washington	Doc Data Sht
Scientific Adviser to MRDC, Thailand	Doc Data Sht
Scientific Adviser Joint	1
Navy Scientific Adviser	Doc Data Sht
Scientific Adviser, Army	1
Air Force Scientific Adviser	1
Director Trials	1
Platforms Sciences Laboratory	
Chief of Airframes and Engines Division	1
Research Leader Propulsion	1
Albert Wong (Head of Helicopter Life Assessment)	1
Frank Polanco (Author)	1
Chris G. Knight (Author)	1
Scott A. Dutton (Author)	1
Phil Ferrarotto (Author)	1
Domenico C. Lombardo	1
Robert Boykett	1
DSTO Libraries and Archives	
Library Fishermans Bend	Doc Data Sht
Library Salisbury	1
Australian Archives	1
Library, MOD, Pyrmont	Doc Data Sht
US Defense Technical Information Center	2
UK Defence Research Information Centre	2

Canada Defence Scientific Information Service	1
NZ Defence Information Centre	1
National Library of Australia	1
Capability Systems Division	
Director General Maritime Development	Doc Data Sht
Director General Aerospace Development	Doc Data Sht
Office of the Chief Information Officer	
Chief Information Officer	Doc Data Sht
Deputy CIO	Doc Data Sht
Director General Information Policy and Plans	Doc Data Sht
AS Information Structures and Futures	Doc Data Sht
AS Information Architecture and Management	Doc Data Sht
Director General Australian Defence Information Office	Doc Data Sht
Director General Australian Defence Simulation Office	Doc Data Sht
Army	
ASNSO ABCA, Puckapunyal	4
SO(Science), DJFHQ(L), MILPO Enoggera, Qld 4051	1
Commander Aviation Support Group, Oakey	1
NAPOC QWG Engineer NBCD c/- DENGRS-A, HQ Engineer Centre Liverpool Military Area, NSW 2174	Doc Data Sht
Air Force	
Director General Technical Airworthiness (Attn OIC RWS), RAAF Williams	3
Director General Policy and Plans, Air Force Headquarters	Doc Data Sht
Director General Technical Air Worthiness, RAAF Williams	Doc Data Sht
Chief of Staff - Headquarters Air Command, RAAF Glenbrook	Doc Data Sht
Commander Aircraft Research and Development Unit, RAAF Edinburgh	Doc Data Sht
Commander Air Combat Group, RAAF Williamtown	Doc Data Sht
Staff Officer (Science), RAAF Amberley	Doc Data Sht
Staff Officer (Science), RAAF Williamtown	Doc Data Sht
Commander Air Lift Group, RAAF Richmond	Doc Data Sht
Commander Maritime Patrol Group, RAAF Edinburgh	Doc Data Sht
Commander Surveillance Control Group, RAAF Williamtown	Doc Data Sht
Commander Combat Support Group, RAAF Amberley	Doc Data Sht
Commander Training, RAAF Williams	Doc Data Sht

Intelligence Program

DGSTA Defence Intelligence Organisation	1
Manager, Information Centre, Defence Intelligence Organisation	1

Corporate Support Program

Library Manager, DLS-Canberra	1

Defence Material Organisation

Chief Engineer, Army Aircraft Logistics Management Squadron	1
Head Airborne Surveillance and Control	Doc Data Sht
Head Aerospace Systems Division	Doc Data Sht
Head Electronic Systems Division	Doc Data Sht
Head Maritime Systems Division	Doc Data Sht
Head Land Systems Division	Doc Data Sht

UNIVERSITIES AND COLLEGES

Australian Defence Force Academy Library (ADFA)	1
Head of Aerospace and Mechanical Engineering, ADFA	1
Deakin University Library, Serials Section (M List), Geelong 3217	1
Monash University, Hargrave Library	Doc Data Sht
Librarian, Flinders University	1

OTHER ORGANISATIONS

NASA (Canberra)	1

OUTSIDE AUSTRALIA

ABSTRACTING AND INFORMATION ORGANISATIONS

Library, Chemical Abstracts Reference Service	1
Engineering Societies Library, US	1
Materials Information, Cambridge Science Abstracts, US	1
Documents Librarian, The Center for Research Libraries, US	1

INFORMATION EXCHANGE AGREEMENT PARTNERS

Acquisitions Unit, Science Reference and Information Service, UK	1
Library – Exchange Desk, National Institute of Standards and Technology, US	1

Inderjit Chopra, Minta-Martin Professor and Director, Alfred Gessow Rotorcraft Center, Aerospace Engineering, University of Maryland, Maryland	1
Charlie Crawford, Chief Engineer, Aerospace and Transportation Laboratory, Georgia Tech Research Institute, Alabama	1
Prof Phil Irving, Head Damage Tolerance Group, School of Industrial and Manufacturing Science, Cranfield University, Cranfield	1
U.S. Army	
Felton Bartlett, US Army Research Laboratory, NASA Langley Research Center (Virginia)	1
Kevin Rotenberger, Aviation and Missile Command (Redstone Arsenal, Alabama)	1
SPARES	5
Total number of copies:	57

DEFENCE SCIENCE AND TECHNOLOGY ORGANISATION DOCUMENT CONTROL DATA				1. CAVEAT/PRIVACY MARKING
2. TITLE Experimental Verification of Helicopter-Rotor Loads-Synthesis Models			3. SECURITY CLASSIFICATION Document (U) Title (U) Abstract (U)	
4. AUTHORS Frank G. Polanco, Chris G. Knight, Scott A. Dutton, and Phil Ferrarotto			5. CORPORATE AUTHOR Platforms Sciences Laboratory 506 Lorimer St, Fishermans Bend, Victoria, Australia 3207	
6a. DSTO NUMBER DSTO–TR–1428	6b. AR NUMBER AR–012–759		6c. TYPE OF REPORT Technical Report	7. DOCUMENT DATE May, 2003
8. FILE NUMBER M1/9/1149	9. TASK NUMBER LRR 02/184	10. SPONSOR DGTA	11. No OF PAGES 28	12. No OF REFS 10
13. URL OF ELECTRONIC VERSION http://www.dsto.defence.gov.au/corporate/reports/DSTO–TR–1428.pdf			14. RELEASE AUTHORITY Chief, Air Vehicles Division	
15. SECONDARY RELEASE STATEMENT OF THIS DOCUMENT *Approved For Public Release* OVERSEAS ENQUIRIES OUTSIDE STATED LIMITATIONS SHOULD BE REFERRED THROUGH DOCUMENT EXCHANGE, PO BOX 1500, EDINBURGH, SOUTH AUSTRALIA 5111				
16. DELIBERATE ANNOUNCEMENT No Limitations				
17. CITATION IN OTHER DOCUMENTS No Limitations				
18. DEFTEST DESCRIPTORS helicopters; rotors; load tests; noise measurement; synthesis; gearboxes				

19. ABSTRACT

Accurately synthesising the load in helicopter-rotor components, using measurements taken from fixed components, has the potential to increase safety and reduce operating costs. Two synthesis models, one of which is able to handle noisy and collinear environments, were validated using data from a Eurocopter Squirrel gearbox fitted to DSTO's Helicopter Transmission Test Facility. The aim of the experiment was to test the models under "challenging" conditions—namely, a noisy and collinear measurement environment. Despite the synthesis techniques being validated, the testing environment did not prove challenging enough (mainly due to insufficient collinearity between the strain gauges). Both the instrumental variable (IV) and least squares (LS) models were able to synthesise the required loads to a high degree of accuracy. The IV model (unlike the LS model) was found to be very sensitive to the chosen gauge combination.